CHARACTERIZATION OF BUBBLE PLUMES IN UNSTEADY CROSS FLOW

Phillype de Lima Massari, phillype.lm@gmail.com
Igor Braga de Paula, igordepaula@puc-rio.br
Pontifical Catholic University of Rio de Janeiro – PUC-RJ, Rua Marquês de São Vicente, 225, Gávea, Rio de Janeiro-RJ, 22451-900, Brazil

Maria Helena Farias, mhfarias@inmetro.gov.br
National Institute of Metrology, Quality and Technology – Inmetro, Av. Nossa Senhora das Graças, 50, Prédio 6, Xerém, Duque de Caxias-RJ, 25250-020, Brazil

Abstract. *This paper presents an experimental investigation of the flow field induced by the interaction between a bubble plume and an oscillating cross flow. Similar flow conditions can be found in artificial aeration processes used for mitigation of pollution contamination in rivers and submarine outfalls in coastal areas. The mixing zone is highly dependent of the flow field near the plume hence the efficiency of aeration processes. In the present work, controlled surface waves were introduced to generate oscillations in streamwise and wall normal components of the cross flow. The waves were excited with a moving paddle and unsteady flow conditions were selected for the investigation. Air was injected in the bottom wall of the water channel to form the bubble plume. Particle Image Velocimetry (PIV) techniques were employed to measure the velocity flow field. Prior to velocity estimation, images were pre-processed using Matlab routines in order to distinguish tracer particles from air bubbles and to create a dynamic mask for the PIV images. Thus, the velocity vector field was estimated using standard PIV algorithms. In addition, properties of the bubbles, such as size and velocity, were also estimated from the acquired images. Finally, the interaction between the bubble plume with the unsteady cross flow was analyzed.*

Keywords*: Air bubble plumes, Surface waves, Unsteady cross flow, PIV, Experimental Study*

1. INTRODUCTION

The dispersion of jets and plumes in stagnant environments and in cross flow have been investigated for many years (Koole and Swan, 1994). Many applications are related with this type of flow, such as air injection in aeration process, discharge of industrial waste floating, oil spill and gas blowout in deep oil wells.

For modeling of pollutant dispersion is necessary to know how does it spread and its mixing characteristics with the environment (Koole and Swan, 1994). Depending on the size of the sources, sinks and chemical interactions, a particle can remain in the environment for many years. This can interfere, damage and promote changes in local ambient. For instance, pollutants emitted by the oil industry in the ocean, can affect marine life and promote significant reduction in population of some species.

Despite the complexity of the problem, some authors have addressed the pollutant dispersion in stagnant and oscillatory environmental conditions, especially for the case of liquid plumes and jets. In the work, of Lam and Xia (2001), a series of laboratory experiments were performed to investigate the behavior of a liquid jet emitted in the presence of oscillatory cross flow. In that work, the amplitude and frequency of the cross flow oscillation were varied systematically in order to study their effects on the jet behavior. An experimental technique was used to create jet oscillations in order to simulate a condition equivalent to an unstable cross flow. This technique was subsequently compared with the technique of generation an unstable environment from a moving paddle. The authors use an instability parameter which represents the degree of cross flow instability. The dispersion characteristics using both techniques were similar in different amplitude and frequencies.

The movement of a horizontal jet exposed to different cross flow oscillations was investigated by Mori and Chang (2003). In that study, Laser-Induced Fluorescence technique (LIF) was used to visualize the flow field and to measure the jet displacement. The experimental conditions were adjusted to maintain the oscillation frequency of the waves constant while the jet velocity and the wave amplitude were varied. The experimental results showed that a phase delay between the jet oscillation and the wave. This delay increased downstream from the injection location. Also the results showed that the jet have not effect on the amplitude of the waves.

Xu et al., (2014) compared mean velocity profiles of a liquid jet in the presence of regular and random waves. They observed a higher dispersion of the jet in the presence of waves when compared with the steady stagnant environment. Their results suggested that waves can enhance mixing. In cases with waves present, they observed wider jets and lower velocities of jet flow in comparison to steady flow. In addition, the movement of the jet was little affected by the forced waves. Koole and Swan, (1994) studied horizontal and vertical liquid jets. In both cases the discharge was done in in the presence of regular and progressive waves. The main flow characteristics were compared with a discharge in stagnant environment. Those comparisons also show a significant effect flow oscillation on the mixing and dilution. In particular, experimental data suggest that a region of most intense fluid mixing is located immediately downstream from the

discharge orifice. Their measurements also suggest that the movement of the waves produced a significant increase in the entrainment of ambient fluid into the jet.

Liu et al., (2005) studied the instantaneous liquid velocity field, flow structures and turbulence caused by different behaviors of air bubble plume in stagnant environment using Particle Image Velocimetry (PIV) techniques. According to their findings, the trajectory of the bubble was affected by liquid viscosity. For low liquid viscosities the bubbles follow a zig-zag trajectory due to vortex pairing of vortices in jet edges. For very low viscosities, a spiral trajectory was observed, inducing the formation of large circular and irregular structures.

According to Zhang and Zhu, (2013), air-water injection is more efficient for artificial aeration, compared to pure water injection. They conducted a study aiming at characterization of air bubble properties in a steady cross flow. Measurements of void fraction, bubble velocity, bubble diameter and interfacial area were performed using an optical fiber sensor. The measurements were performed at different sections along the air bubble trajectory. The results were compared with other studies in stagnant environment. It was observed that the bubble velocity distribution did not follow a Gaussian profile. In addition, the bubble velocity increased downstream from the injector.

Recently, laboratory experiments were conducted by Wang and Socolofsky (2015) to measure the bubble dynamics in stagnant and steady cross flow. Image processing techniques were adopted to measure the bubble contour. Bubbles were distinguished from background images using an edge detection and threshold algorithm. Raw images were converted to binary images and the instantaneous rising velocity was calculated by tracing the vertical displacement of the center of the bubble detected during the time between two consecutive frames. To measure the bubble size, the circular area equivalent diameter of the bubbles was computed to match the projected area of each bubble in the binarized images. Thereby, they could successfully measure bubble velocities.

Jets and plumes are considered of practical importance in various applications such as hydraulic, mechanical, aerospace, environmental, chemical engineering, among others. Few studies have been conducted considering bubble plumes in crossflow. Yet, no investigation was found in the literature to address the problem of bubble plumes in oscillatory cross flow. Considering the aforementioned facts, it is important to investigate this case due to its practical relevance. Therefore, the present work focuses on the investigation of bubble plumes dispersion in an unsteady environment. An experimental investigation is carried out to characterize the bubble plume and its interaction with controlled waves.

3. EXPERIMENTAL SET-UP

The experiments were carried out in the National Institute of Metrology, Quality and Technology – Inmetro – in a water channel (Figure 1) with 12 m long, 0.6 m wide and 0.7 deep. All the side walls and bottom of the channel was constructed using glass for optical access. A centrifugal pump of 30 kW power is used to moves the water in the channel, allowing a maximum flow rate of 648 m^3/h. For monitoring the flow, an electromagnetic flowmeter is installed downstream of the pump.

Figure 1. Water channel

The schematic drawing of the experimental setup is shown in Figure 2. In the entry channel section there are flow rectifiers and stainless steel screens. To perform the air injection into the channel, it was necessary to place a false bottom above the original bottom made of glass. A hose was connected to the air injector through all the false bottom to the channel exit section, where there is a mass flow meter type allowing control of the air injection velocity.

To reproduce the oscillatory cross flow, a wave generator was designed and assembled. The wave generator is composed of a servo motor that has the rotary motion converted into linear movement and an acrylic plate enters and leaves on the water surface, generating waves. To reduce the reflection of the waves, it was placed an inclined plate like a beach in the exit section of the water channel.

The velocity field was measured using standard Particle Image Velocity techniques (PIV). The PIV system used in this work was the LaVision, composed of a pulsed Laser Nd: YAG dual cavity, one CCD camera dual frame with 50 mm lens and two low-pass filter of 532 nm and 540 nm. The laser was inclined in 46 ° from the horizontal to light all the bubble plume field of view. The CCD camera was placed in a structure with vertical and horizontal positioners to enable the displacement on the axes and pointed perpendicularly to the laser illumination plane. A pulsed Led was synchronized with the laser on the Q-switch trigger (Figure 3) and placed on the opposite side of the camera, so that when the laser

pulses the Led receives a signal to expose the light, so that the bubbles keep visible due to the shadow created by the Led light exposure. On the standard parameters of the double frame mode, the first frame exposure time was set as 5µs, so the Led light could not illuminate the first frame of the camera. Therefore, the first frame exposure was increased to 90µs. As the bubbles scatter light at the same wavelength of laser light (532 nm), it was necessary to use a low pass filter of 540 nm in the camera and fluorescent tracer particles. It was decided to use rhodamine for measurements with the presence of the plume of bubbles. And for base flow characterizing, the particles used were the silver hollow glass spheres.

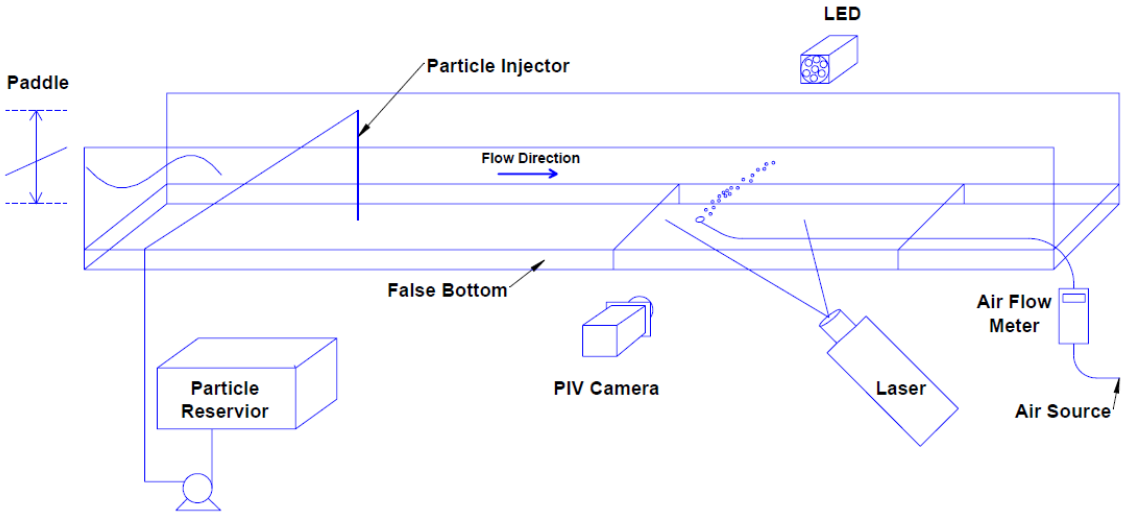

Figure 2. Schematic of experimental setup

Due to the high volume of water in the channel, it was not convenient to seed the whole tunnel with tracing particles. Therefore, it was designed a particle injection system where tracer particles were inserted in the channel only when the PIV system is in use.

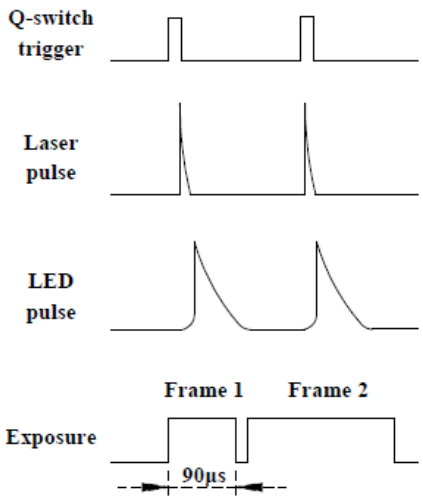

Figure 3. Led synchronization scheme

The laser light sheet of the system PIV illuminates the centerline of the bubble plume region. However, the camera field of view is smaller than the whole plume region. Therefore, the camera had to be displaced to cover all the region of interest. In total, nine windows were necessary to cover the plume area, as illustrated schematically in Figure 4. One camera field of view has dimensions approximately by 125 x 95 mm. In the figure, the vertical window displacement is referenced with the letters A, B and C, while the horizontal displacement is represented with the numbers 1, 2 and 3. Within the measurements, the water level was kept constant at 300 mm. In addition, only a single nozzle with 1 mm in diameter was tested.

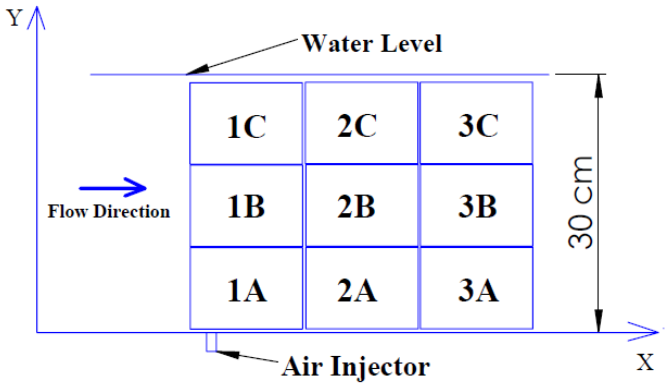

Figure 4. Fields of view

The experimental conditions covered in this study are shown in Table 1. For these set of experiments, two different wave amplitudes and a single wave frequency are analyzed. The cross flow velocity was not varied within the current experiments. The idea is to observe only the effect of the wave amplitude on the bubble dispersion. Initially, the air speed was also kept constant. A low velocity was chosen because it produces well-spaced air bubbles. Thus, algorithms developed for identification of bubble contours can be accurately validated.

Table 1. Experimental conditions

Water Flow Rate (m^3/h)	Air Flow Rate (L/min)	Wave Amplitude (cm)	Wave Frequency (Hz)
92	0.2	1.0	0.67
		2.0	

4. IMAGE DATA PROCESSING

For the bubbles properties evaluation, it was necessary to carry out pre-processing of the raw images obtained by the PIV technique. Matlab routines were used to process the images acquired. The code was designed aiming at the identification of the region occupied by the bubbles. Thereby, dynamic masks can be created. This allows to distinguish air bubbles from tracer particles in the images.

The image processing algorithm is divided into three parts. The first is related to the image pre-processing. In this part, all the raw images acquired by PIV technique are cropped into a region of interest. A conversion of the original RGB images to grayscale is applied and a median filter of size 7 x 7 pixels is used to remove the particles from the images. Due the light emitted by the Led, the lighting of the images has a non-uniformity, they are brighter in the center and darker at the edges. To correct the background illumination, a similar background is taken, based on the original image histogram, as a separate image, then, this approach has been subtracted from the original image. Finally, a global threshold is used to convert the intensity image to a binary one. In the binarized image, regions occupied by bubbles have pixel values equal to 0 (black area) and the remaining pixel values are equal to 1 (white area). Standard open and close functions are used to fill bubble regions that still had holes due to light reflection. Figure 5 shows the steps sequence of image processing.

After identifying the regions of the bubbles, dynamic masks were created for each bubble in the image acquired by the PIV system. The original image was multiplied with the inverted binaries image, so that the pixels on the bubble regions remain with values equals zero and all the other pixel regions remain as the same aspect of the original image. Thus, the pre-processed images are sent back to the standard PIV software and processed.

The second part of the code is devoted to evaluate properties of the bubbles. The binarized images undergo a function that paint each bubble region with different pixel intensity. Thus, each bubble can be distinguished from each other. In a sequence, a contour is generated around each bubble and a number is added for a quick identification. Thus, it is estimated area, perimeter, centroid coordinates and diameter for each bubble.

The third part of the code evaluates the bubble velocity. In this part, images from each PIV exposure are used. In the code, the bubble centroid positions in the first and second PIV images are identified and the distance between the two points of the centroids is calculated. Since the time between the two images exposures is known, it is possible to calculate the bubble rise velocity.

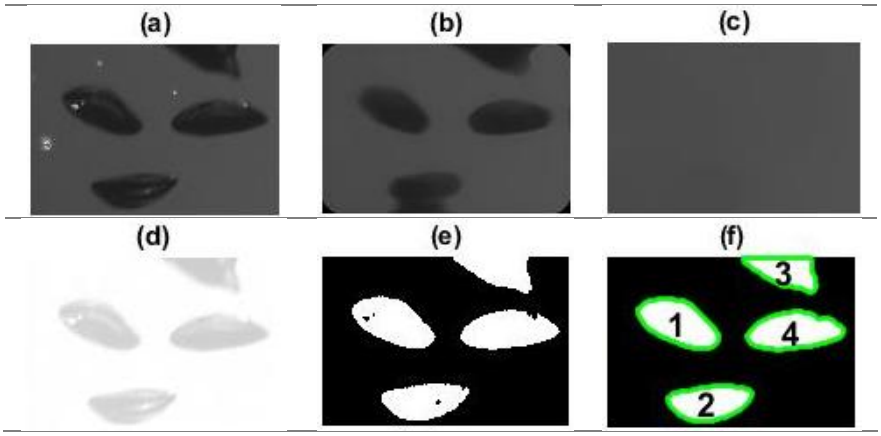

Figure 5. An example of the image processing sequence. **(a)** Show the original image. **(b)** Pass a median filter to remove tracer particles. **(c)** Obtain the background. **(d)** Represent the image **(b)** subtracted from the background. **(e)** Detection of bubbles areas with a dynamic threshold. **(f)** Imposes boundaries and list the amount of bubbles in the image

5. RESULTS

5.1 Base Flow Characteristics

In the Figure 6, the velocity vector field is depicted for characterization of the base flow without the presence of bubbles. The vector field displayed in Fig. 6 is an average of 400 vector fields. The presented results are acquired at all nine field of view at the flow rate of 92 m^3/h without the presence of waves. The results obtained for waves conditions are similar, whereas that the vector field is obtained from the mean velocity.

It can be observed that the velocity profile is uniform in all cases. It can also be observed that the color gradient indicates the boundary layer. As expected, the velocity is higher on the top of the field of view due the free surface.

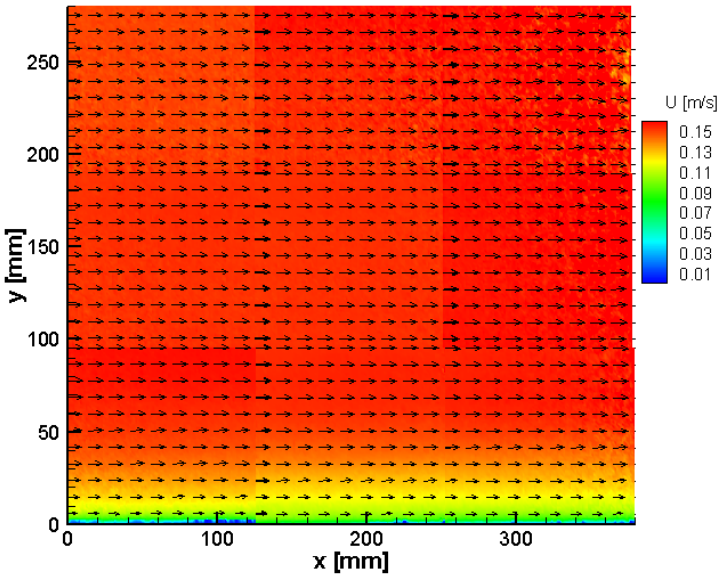

Figure 6. Velocity vector field of the base flow characterization for all field of view

For the boundary layer thickness analysis, the velocity data obtained by PIV technique were plotted versus water deep. Figure 7 shows the velocity variation along the height for positions 1A, 1B and 1C, without wave conditions, with wave amplitude of 1 cm and wave amplitude of 2 cm. It is observed that, for flow conditions without the presence of waves, the boundary layer thickness is approximately 10 cm, with laminar boundary layer characteristics. In the conditions with waves, there is a slight delay in the boundary layer formation, and in both wave cases the thickness is about 15 cm.

Away from the bottom channel, the velocity points seem to disperse more clearly, however, the velocity variation is negligible.

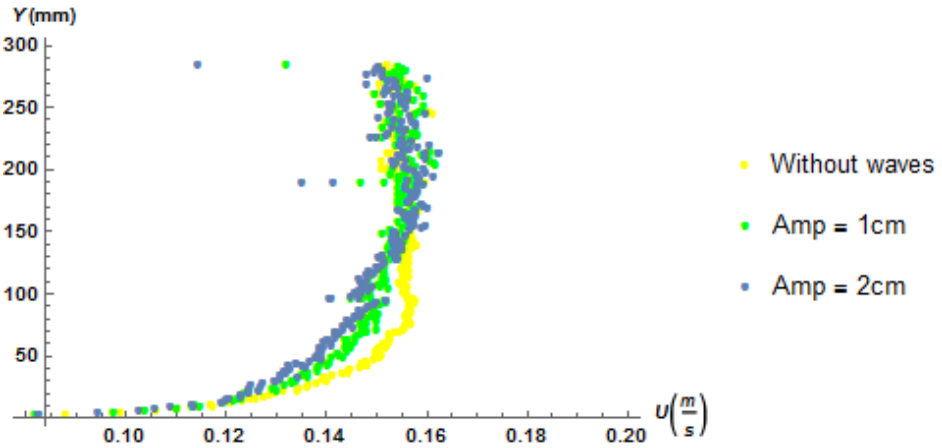

Figure 7. Velocity profile for different conditions

5.2 Bubble Diameter

The bubbles diameters were estimated based on two approaches. The first method evaluates the area (A) of the region occupied by the bubble in the code implemented in Matlab. With the calculated area, it is possible to determine equivalent circular diameter ($D_{circular}$) that is estimated based on Eq. 1.

$$D_{circular} = \sqrt{\frac{4A}{\pi}} \tag{1}$$

The second method is based on the premise that most of the bubbles have approximately an ellipse shape. Thus, the code identifies the major axis (a) and minor axis (b) of the elliptical region. The diameter ($D_{elliptic}$) calculated on Eq. 2 is established from the volume of an ellipsoid (Wang and Socolofsky, 2015).

$$D_{elliptic} = (ab^2)^{1/3} \tag{2}$$

All binarized images were processed so that the regions of pixels equal to 0 (black) represent the image background and regions with pixel values equal to 1 (white) represent the bubbles. However, during the analysis process, which is an automatic identification of some bubbles, the system computed regions containing bubbles very close to each other as being a single bubble. Moreover, some particles that were not removed completely by the filter, were also identified as very small bubbles. To solve this problem, it was adopted a criterion for removing the regions containing these errors.

The outlier criterion was based on the calculated diameters. It was analyzed 20% of the images manually. Evident bubbles region was identified and computed as valid diameters. Thus, it was determined a diameter range corresponding to regions which had individual bubbles. Only bubbles with diameter values between 3.5 mm $\leq D_{circular/elliptic} \leq$ 6.0 mm, were accounted for analysis.

Figure 8 shows the relationship between the two methods of evaluating the diameter. All points on the graph represent the bubbles of 400 images analyzed from a single frame with the respective equivalent diameters calculated by the code. The solid diagonal line represents the equivalence between the two diameters ($D_{circular} = D_{elliptic}$). The red dotted line represents the best fit for the number of samples acquired: $D_{circular} \approx 0.87 D_{elliptic}$. The mean of $D_{circular}$ is of 5.0 mm with standard deviation of ± 0.53 mm, while $D_{elliptic}$ has a mean equal to 4.5 mm and standard deviation of ± 0.51 mm. Standard deviations are depicted in error bar for the circular and elliptic equivalent diameter.

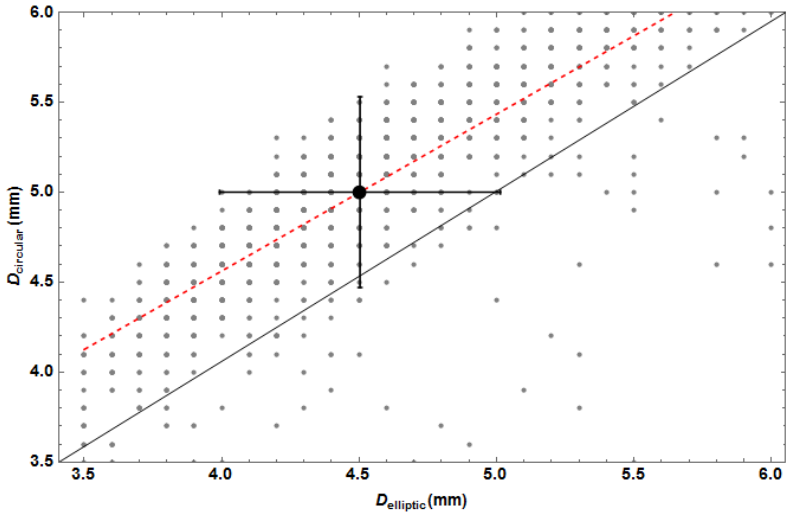

Figure 8. Relation between diameters

Considering the adopted criteria, it is possible to realize in the graph that the values of equivalent circular diameters calculated by the method is slightly larger than the equivalent elliptic diameter, as also seen in the work of Wang and Socolofsky (2015). It is evident from the sample images that bubbles have predominantly elliptical shape, so the bubbles velocity analyzes were performed based on the equivalent elliptic diameter ($D_{elliptic}$).

5.3 Bubble Rise Velocity

To determine the bubble rise velocity (V_B), two consecutive frames of each binarized image was sent to a specific code. In this algorithm, the centroid of the region bounded by each bubble has been identified for the two frames. The distance between the two points corresponding to the same centroid bubbles in each frame was calculated from a function that obtains the Euclidean distance between two points. To ensure that the distance between the two centroids corresponding to the same bubbles in frame 1 and frame 2, a criterion in the code was adopted, this one requires that only minimum distances are calculated between each centroid. This is done by an iteration between each centroid identified in the images.

After calculating the Euclidean distance between the two centroids, the results were divided by the time between the two laser pulses (5 ms), since they correspond to the time of acquisition of two frames. Figure 9 shows the velocity variation along the height for position 2C for 400 images.

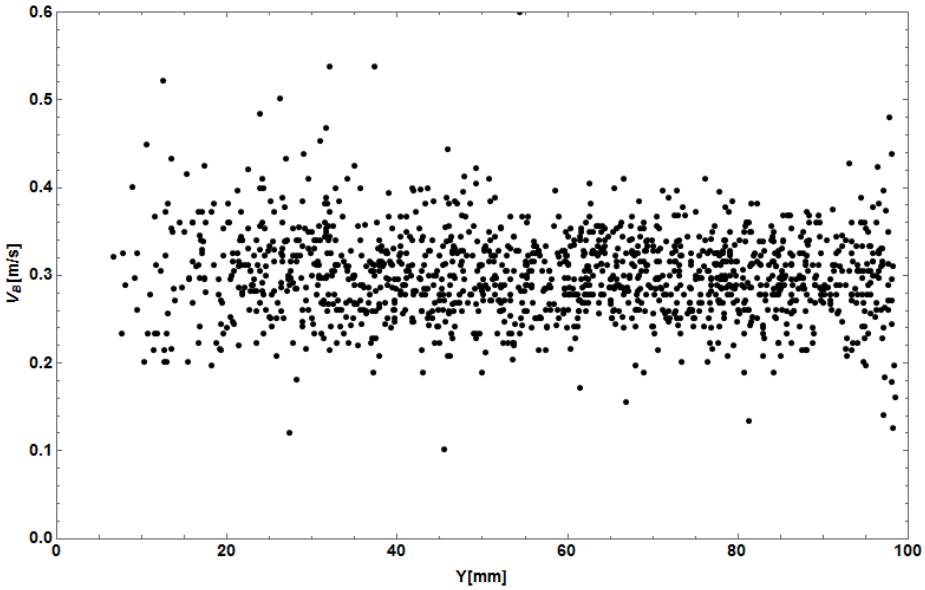

Figure 9. Bubble velocity versus height on the field of view 2C

It can be observed on the Fig. 9 that the velocity does not vary significantly along 95 mm. Considering the cross flow velocity as 0.15 m/s at this field of view, it is consistent to have bubbles velocities higher than the main velocity of cross flow due to the initial air injection velocity and buoyance effect.

6. CONCLUSIONS

The present work allowed the beginning of a study on the interaction of oscillatory cross flow with the presence of air bubble plume. The image processing methodology proved to be valid for distinguishing the air bubbles from the tracer particles immersed in a fluid. Also, it was appropriate to determine the diameters of the bubbles and the velocity, although the automation code has sometimes confused bubbles with particles.

Further analysis will be made to evaluate the conditions with waves with an application of a Proper Orthogonal Decomposition method (POD) to separate the waves energetics modes, so it can enable more accurate observations about wave effects on the flow.

7. ACKNOWLEDGEMENTS

The authors are grateful to CNPq, PUC-Rio and INMETRO for their support and sponsorship which have become possible the development of this research.

8. REFERENCES

Dhanak, M., Xiros, N. I., 2017. “Marine Oufalls”. Handbook of Ocean Engineering, Part C. pp. 7-36, Springer-Verlag.

Koole, R. and Swan, C., 1994. “Dispersion of pollution in a wave environment”. Coastal Engineering, Chapter 221, pp. 3071-3085.

Lam, K. M. and Xia, L. P., 2001. “Experimental simulation of a vertical round jet issuing into an unsteady cross-flow”. Journal of Hydraulic Engineering, Vol. 127, No. 5, pp. 369-379.

Liu, Z., Zheng, Y., Jia, L., Zhang, Q., 2005. “Study of bubble induced flow structure using PIV”. Chemical Engineering Science, pp. 3537-3552.

Mori, N. and Chang, K., 2003. “Experimental study of a horizontal jet in a wave environment”. Journal of Engineering Mechanics, Vol. 129, No. 10, pp. 1149-1155.

Xu, Z., Chen, Y., Zhang, C., Li, C., Wang, Y., Hu, F., 2014. “Comparative Study of a vertical round jet in regular and random waves”. Journal of Ocean Engineering, pp. 200-210.

Wang, B. and Socolofsky, S. A., 2015. “On the bubble rise velocity of a continually released bubble chain in still water and with crossflow”. Physics of Fluids, Vol. 27, pp. 103301-1 – 103301-20.

Zhang, W. and Zhu, D. Z., 2013. “Bubble characteristics of air-water bubbly jets in crossflow”. International Journal of Multiphase Flow, pp. 156-171.

9. RESPONSIBILITY NOTICE

The authors are the only responsible for the printed material included in this paper.